ACTA MONTANA IGt CSAS (1992)
Series A, No. 1(87), 33—56

NUMERICAL TESTING AND COMPARISON OF CONSTITUTIVE MODELS OF GEOMATERIALS

MARTA DOLEŽALOVÁ, ZDENĚK BOUDÍK and IVO HLADÍK

Institute of Geotechnics, Czechoslovak Academy of Sciences,
V Holešovičkách 41, 182 09 Prague, Czechoslovakia

Abstract: Numerical testing and graphical representation of hypoelastic constitutive relations of geomaterials using numerical element tests and unit stress response envelopes of Gudehus (1979). Derivation of basic relations and comparison of five models: isotropic linear elastic, transversely isotropic, hyperbolic with different switch functions, path dependent variable moduli and elastoplastic (Cam clay) model with hardening.

Key words: constitutive relation; hypoelasticity; path dependence; stress response; elastoplasticity; hardening; geomaterial

1. INTRODUCTION

According to Truesdell's definition (1984) constitutive relations embody the distinguishing properties of materials and transform the history of an arbitrary thermokinetic process given by motion, temperature and time into a calorodynamic process determined by stress, motion, body force, internal energy, entropy, heating and time. The constitutive equations complement the fundamental laws of physics in solving boundary value problems of thermodynamics. In nonlinear continuum mechanics and geomechanics definitions in the narrow sense are used. The equations relating the internal forces in a material to the motion of the material are called constitutive equations (Leigh, 1968) and the relations between the stress tensor, strain tensor and time are denoted as constitutive laws (models) of geomaterials (Feda, 1982).

The constitution of a physically correct set of these material laws is considered to be the fundamental task of geomechanics in general and the key problem of efficient application of numerical methods in this field in particular.

The recent rapid development in constitutive modelling of geomaterials has already produced a large number of models (Gudehus *et al.*, 1984; Murayama, 1984; Beer *et al.*, 1991) which have not yet been properly compared, evaluated and selected. This requires, in the first place, the basic requirements to the constitutive relations to be specified and the way of numerical testing to be outlined. A comprehensive checklist of the requirements to the constitutive models of geomaterials has already been published by Gudehus (1985). Along with the engineering aspects (the processes and properties to be covered, the manageability of the relations) the

mathematical (existence, convergence, uniqueness and stability of the solution) and physical principles (determinism, causality, objectivity, local action, consistency) should be implied by any relevant constitutive model.

The principle of determinism is of particular importance for geomaterials. It states that every phenomenon is determined totally by the history or sequence of causes. Thus the magnitude of stress and deformation in a body due to an external force depends on the past history of the external forces experienced by the body. During the loading of soils and rocks irreversible deformation and change of their structure occur due to dissipation of mechanical energy. Accordingly, the stresses and strains in soil depend on the sequence of loading states and structural changes, i.e. they are path dependent. Such behaviour can be only described by incremental constitutive equations subsequently integrated along the particular stress paths. The use of the finite form of constitutive relations for geomaterials is highly limited or even impossible.

The incremental, path dependent constitutive relations can be, from the theoretical standpoint, effectively checked by so-called numerical element test, i.e. by numerical experiments with a soil sample under uniform stress and strain (Gudehus, 1985; Gudehus and Kolymbas, 1985). In this way one can systematically explore the existence, convergence and uniqueness of any particular constitutive law together with its manageability and physical correctness. Any simple or complex stress and strain path, loading history, including paths of standard and non-standard laboratory tests, can be followed by means of numerical integration.

In this paper axially symmetric, triaxial numerical tests are used for testing some selected hypoelastic constitutive relations. The incremental unit response of the linear isotropic and transversely isotropic materials are presented in the first part of the paper using a special graphics (Gudehus, 1979). Then the responses of the hyperbolic and path dependent variable moduli relations are compared for the Karlsruhe sand. The next part of the paper is devoted to the numerical testing of elastoplastic constitutive models with hardening. The basic relation for the so-called critical state or Cam clay model (Roscoe *et al.*, 1958) and the numerical procedures necessary for their implementation at a stress point are presented, and the unit response is calculated. It should be noted that the evaluation and understanding of the Cam clay model response is of particular importance as it forms a basis for many other widely applied elastoplastic models of soils. Finally, the responses of the tested constitutive models are compared and a plan for further research outlined.

2. NUMERICAL TESTING OF HYPOELASTIC CONSTITUTIVE RELATIONS

The concept of hypoelasticity introduced by Truesdell constitutes a generalized incremental law in which the increment of stress tensor $\dot{\sigma}_{ij}$ is a function of stress tensor σ_{kl} and increment of strain tensor $\dot{\varepsilon}_{kl}$ (Desai and Siriwardane, 1984; Bojtár, 1988):

$$\dot{\sigma}_{ij} = f_{ij}(\sigma_{kl}, \dot{\varepsilon}_{kl}) \tag{2.1}$$

For time independent materials Eq. (2.1) should be homogeneous in time (all terms containing exponents of $\dot{\varepsilon}_{kl}$ higher than one are eliminated), and the incremental form of Eq. (2.1) can be obtained by integration in time. The general linear relation between the stress increment and strain increment then reads

$$\mathrm{d}\sigma_{ij} = C_{ijkl}\mathrm{d}\varepsilon_{kl} \tag{2.2}$$

where the tangent stiffness tensor C_{ijkl} is a function of the stress tensor only. The general hypoelastic model given by Eq. (2.2) requires 12 response functions $\alpha_0, \ldots, \alpha_{11}$, which depend on the stress invariants:

$$\begin{aligned}\mathrm{d}\sigma_{ij} = {} & \alpha_0 \mathrm{d}\varepsilon_{kk}\delta_{ij} + \alpha_1 \mathrm{d}\varepsilon_{ij} + \alpha_2 \mathrm{d}\varepsilon_{kk}\sigma_{ij} + \alpha_3 \sigma_{mn}\mathrm{d}\varepsilon_{nm}\delta_{ij} + \\ & + \alpha_4(\sigma_{im}\mathrm{d}\varepsilon_{mj} + \mathrm{d}\varepsilon_{im}\sigma_{mj}) + \alpha_5 \mathrm{d}\varepsilon_{kk}\sigma_{im}\sigma_{mj} + \alpha_6 \sigma_{mn}\mathrm{d}\varepsilon_{nm}\sigma_{ij} + \\ & + \alpha_7 \sigma_{mn}\sigma_{nk}\mathrm{d}\varepsilon_{km}\delta_{ij} + \alpha_8(\sigma_{im}\sigma_{mk}\mathrm{d}\varepsilon_{kj} + \mathrm{d}\varepsilon_{im}\sigma_{mk}\sigma_{kj}) + \\ & + \alpha_9 \sigma_{mn}\mathrm{d}\varepsilon_{nm}\sigma_{ik}\sigma_{kj} + \alpha_{10}\sigma_{mn}\sigma_{nk}\mathrm{d}\varepsilon_{km}\sigma_{ij} + \\ & + \alpha_{11}\sigma_{mn}\sigma_{nk}\mathrm{d}\varepsilon_{km}\sigma_{ir}\sigma_{rj}\,; \end{aligned} \tag{2.3}$$

here δ_{ij} is the Kronecker delta (1 for $i = j$ and 0 for $i \neq j$).

Due to their incremental nature the hypoelastic models have a greater generality than the hyperelastic models, and they allow not only for nonlinear but also for inelastic (i.e. plastic) behaviour including path dependenence, induced anisotropy, dilatancy and many other important features of geomaterials. The hypoelastic models, however, reveal certain reversibility to infinitesimal stress increment removal. This is the reason for using the word "hypo", which means "in a lower sense". Hypoelastic material is only elastic in a lower, i.e. incremental sense.

The general relation with 12 response functions can be used to obtain hypoelastic laws of different orders. If the right-hand side of Eq. (2.3) is stress independent, then only two parameters will be retained, and the zero-order hypoelasticity, i.e. the incremental form of Hooke's law, obtained. This is the basis for different incrementally linear variable moduli models including the path dependent model (Doležalová, 1985) and the well-known hyperbolic model of Duncan and Chang (1970). Assuming linear stress dependence of the right-hand side of Eq. (2.3), seven parameters will be retained and the first-order hypoelastic law obtained. It can be shown that any incrementally linear elastoplastic relation (compare Eqs. (2.2) and (4.9)) and even incrementally nonlinear rate type relations (Kolymbas, 1987) can be treated as special cases of hypoelasticity (Bojtár, 1988).

The numerical element tests with uniform stresses and strains of the sample and the unit stress response envelope suggested by Gudehus (1979) are powerful tools for numerical testing of incremental type, path dependent laws. The basic idea is to impose a unit strain increment of various directions on the soil sample and to calculate the corresponding stress response according to the tested constitutive law.

For the sake of simplicity axially symmetric stress state ($\sigma_1, \sigma_2 = \sigma_3$ or $\sigma_3, \sigma_1 = \sigma_2$, if generally principal stresses $\sigma_1 > \sigma_2 > \sigma_3$) is supposed and the cylindrical soil

sample is loaded by unit strain rate defined as $\sqrt{\dot{\varepsilon}_1^2 + 2\dot{\varepsilon}_2^2} = \text{const.}$ ($\dot{\varepsilon}_1, \dot{\varepsilon}_2 = \dot{\varepsilon}_3$ are principal strain rates). The strain rate is fully described by its direction

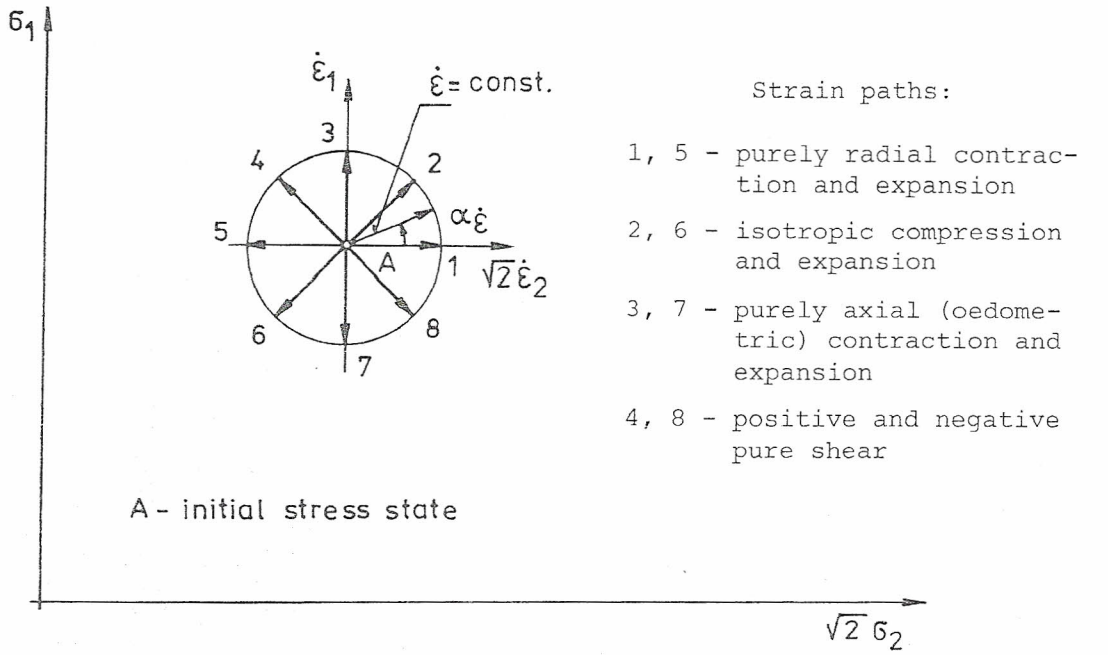

Fig. 1. Strain paths with constant strain increment $\dot{\varepsilon}$ (after Gudehus, 1979).

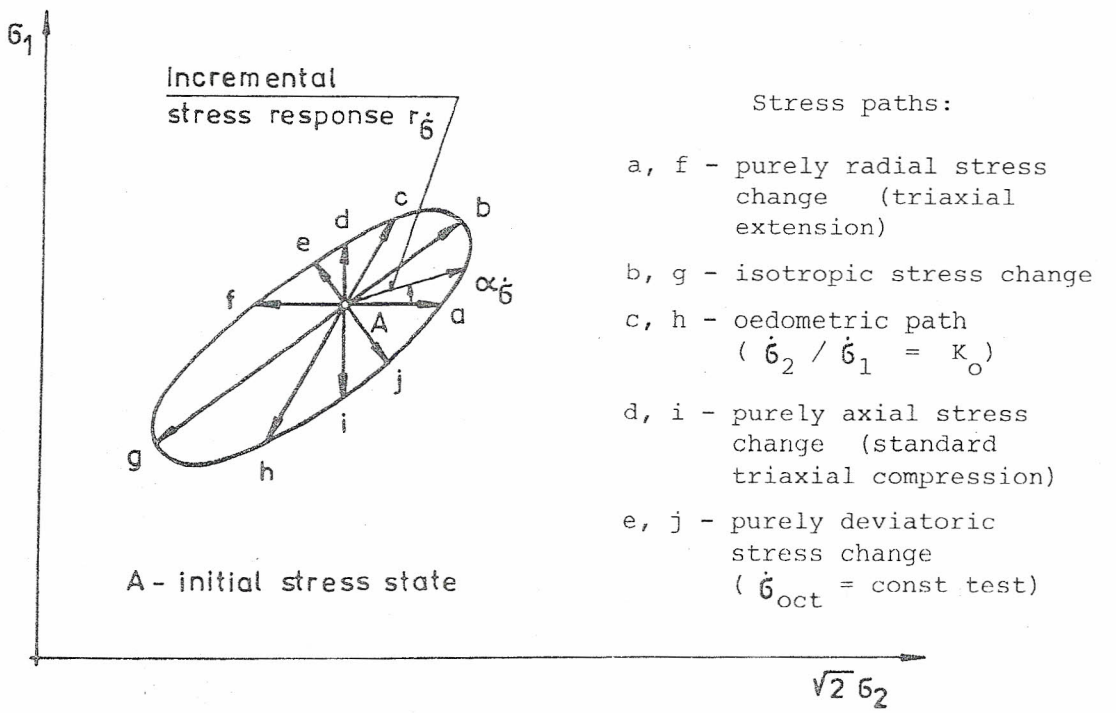

Fig. 2. Incremental stress response $r_{\dot{\sigma}}$ corresponding to constant strain increment $\dot{\varepsilon}$ (after Gudehus, 1979).

$\alpha_\varepsilon = \arctan(\dot{\varepsilon}_1/\sqrt{2}\,\dot{\varepsilon}_2)$ (Fig. 1). The stress rate response is represented by a polar diagram of intensities $r_{\dot{\sigma}} = \sqrt{\dot{\sigma}_1^2 + 2\dot{\sigma}_2^2}$ and directions $\alpha_{\dot{\sigma}} = \arctan(\dot{\sigma}_1/\sqrt{2}\,\dot{\sigma}_2)$ in the diagonal plane $\dot{\sigma}_1$ vs. $\sqrt{2}\,\dot{\sigma}_2$ (Fig. 2). Generally $\alpha_{\dot{\varepsilon}} \neq \alpha_{\dot{\sigma}}$, and directional coincidence is only achieved at the maximum and minimum responses ($\alpha_{\dot{\varepsilon}_p} = \alpha_{\dot{\sigma}_p}$, see Eqs. (3.3) – (3.4)) for the zero order hypoelastic laws and the incrementally linear rate type relations. Since all relations tested are homogeneous in time, the overdot in the above and subsequent relations means simply an incremental quantity.

3. LINEAR, BILINEAR AND MULTILINEAR HYPOELASTIC RESPONSE

3.1. Linear response

Linear response is produced by an incrementally linear law without switch functions.

The linear relationship for the axisymmetric case can be formulated as

$$\begin{aligned} \dot{\sigma}_1 &= M_{11}\dot{\varepsilon}_1 + M_{12}\sqrt{2}\,\dot{\varepsilon}_2 \\ \sqrt{2}\,\dot{\sigma}_2 &= M_{21}\dot{\varepsilon}_1 + M_{22}\sqrt{2}\,\dot{\varepsilon}_2 \end{aligned} \tag{3.1}$$

where coefficients M_{ij} are independent of direction $\alpha_{\dot{\varepsilon}}$. The material is called hypoelastic if the M_{ij} depend on stress only. One can rewrite equations (3.1)

$$\begin{aligned} r_{\dot{\sigma}} \sin\alpha_{\dot{\sigma}} &= M_{11} \sin\alpha_{\dot{\varepsilon}} + M_{12} \cos\alpha_{\dot{\varepsilon}} \\ r_{\dot{\sigma}} \cos\alpha_{\dot{\sigma}} &= M_{21} \sin\alpha_{\dot{\varepsilon}} + M_{22} \cos\alpha_{\dot{\varepsilon}} \end{aligned} \tag{3.2}$$

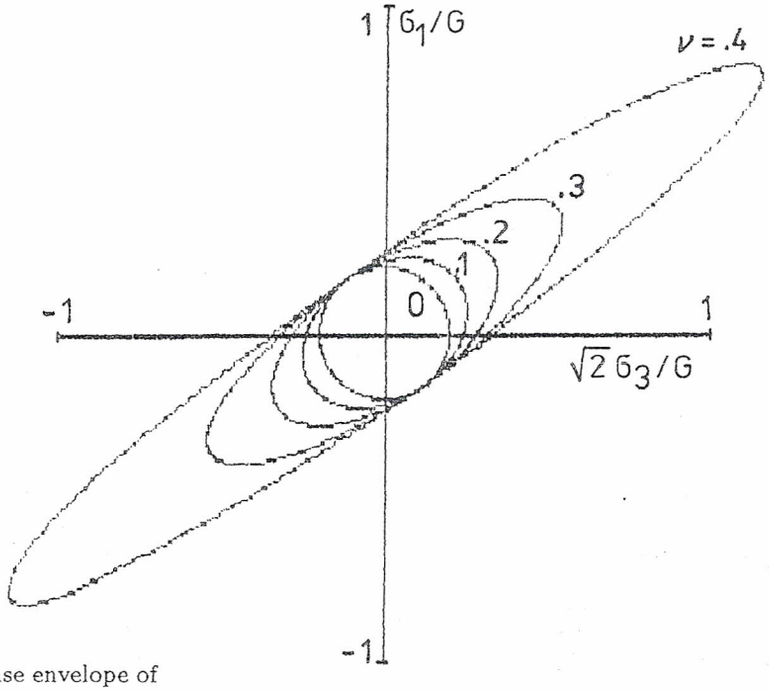

Fig. 3. Response envelope of a linear isotropic material with different Poisson ratios ν.

The response envelope associated with equations (3.2) can be shown to be an ellipse (Fig. 3) provided that

$$\det M_{ij} = M_{11}M_{22} - M_{21}M_{12} > 0\,.$$

This ellipse is completely defined by M_{ij} as supported by the following four relationships:

$\alpha_{\dot{\varepsilon}_p}$, strain rate direction associated with maximum or minimum intensity $r_{\dot{\sigma}}$ of stress rate response, given by

$$\tan 2\alpha_{\dot{\varepsilon}_p} = 2\,\frac{M_{11}M_{12} + M_{21}M_{22}}{M_{12}^2 + M_{22}^2 - M_{11}^2 - M_{21}^2} \tag{3.3}$$

$\alpha_{\dot{\sigma}_p}$, stress rate direction of maximum or minimum intensity of stress rate response, given by

$$\tan 2\alpha_{\dot{\varepsilon}_p} = 2\,\frac{M_{11}M_{22} + M_{21}M_{11}}{M_{22}^2 + M_{21}^2 - M_{12}^2 - M_{11}^2} \tag{3.4}$$

maximum and minimum intensities of stress response

$$r_{\dot{\sigma}_p} = \sqrt{(M_{11}\sin\alpha_{\dot{\varepsilon}_p} + M_{12}\cos\alpha_{\dot{\varepsilon}_p})^2 + (M_{21}\sin\alpha_{\dot{\varepsilon}_p} + M_{22}\cos\alpha_{\dot{\varepsilon}_p})^2} \tag{3.5}$$

with the two solutions $\alpha_{\dot{\varepsilon}_p}$ of equation (3.3).

For a symmetric response matrix, i.e. $M_{12} = M_{21}$, one obtains $\alpha_{\dot{\varepsilon}_p} = \alpha_{\dot{\sigma}_p}$ from equations (3.3) and (3.4). The case of isotropic loading is defined by

$$\alpha_{\dot{\sigma}_p} = \alpha_{\dot{\varepsilon}_p} = \arctan\left(\frac{1}{\sqrt{2}}\right) = 35.3^\circ \tag{3.6}$$

In this case the coefficients M_{ij} can be expressed from general Hooke's law in terms of Young's modulus of elasticity E and Poisson's ratio ν

$$\begin{aligned} M_{11} &= \frac{E}{2(1+\nu)}\,\frac{2(1-\nu)}{(1-2\nu)}\,; \\ M_{22} &= \frac{E}{2(1+\nu)}\,\frac{2}{(1-2\nu)}\,; \\ M_{12} = M_{21} &= \frac{E}{2(1+\nu)}\,\frac{2\sqrt{2}\,\nu}{(1-2\nu)}\,. \end{aligned} \tag{3.7}$$

The shape of ellipses is determined by ν only (Fig. 3). $\nu = 0$ ($M_{11} = M_{22}$) yields a circle. $\nu = .5$ yields a pair of straight lines.

In the case of transverse isotropy, when e.g. the cylindrical test sample is horizontally layered, coefficients M_{ij}, expressed from general Hooke's law, are evaluated from equations (3.8). Material constants E_1, ν_1 (G_1 is dependent) are associated with the behaviour in the plane of strata and E_2, ν_2 (G_2 is independent, but it does not influence the case under consideration) with the direction normal to the strata.

$$M_{11} = \frac{E_2}{(1+\nu_1)(1-\nu_1-2n\nu_2^2)}(1-\nu_1^2); \quad n = \frac{E_1}{E_2}$$
$$M_{22} = \frac{E_2}{(1+\nu_1)(1-\nu_1-2n\nu_2^2)} n(1+\nu_1) \tag{3.8}$$
$$M_{12} = M_{21} = \frac{E_2}{(1+\nu_1)(1-\nu_1-2n\nu_2^2)} \sqrt{2}\, n\nu_2(1+\nu_1)$$

The response envelope of a real transversely isotropic material, whose material constants satisfy thermodynamic conditions, is shown in Fig. 4.

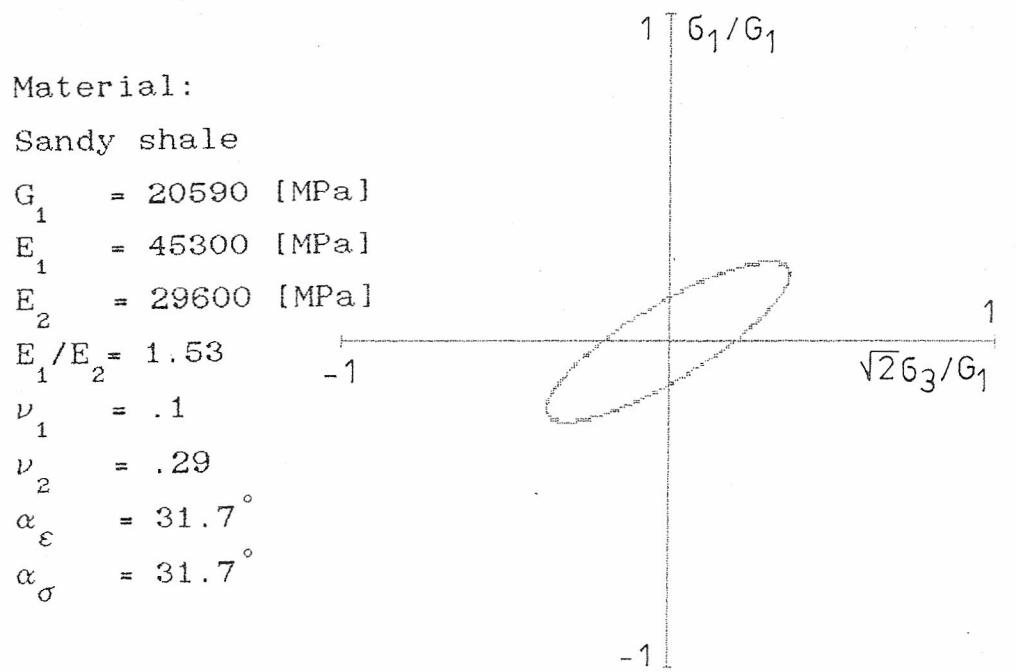

Fig. 4. Response envelope of linear transversely isotropic material with $n = E_1/E_2 = 1.53$ and $\nu_1/\nu_2 = 0.345$.

3.2. Bilinear response

Bilinear response is given by one switch function separating the cases of loading and unloading. This behaviour can be demonstrated by the hyperbolic model using different moduli for loading and unloading.

The hyperbolic model is based on the assumption of hyperbolic relation between axial strain ε_1 and deviatoric stress $(\sigma_1 - \sigma_3)$ during the standard triaxial test that can be expressed by the relation suggested by Kondner (1963):

$$\sigma_1 - \sigma_3 = \frac{\varepsilon_1}{a + b\varepsilon_1} \tag{3.9}$$

Duncan and Chang (1970) derived, from this relationship, the Mohr-Coulomb failure criterion expressed as

$$(\sigma_1 - \sigma_3)_{\mathrm{f}} = \frac{2c\cos\phi + 2\sigma_3 \sin\phi}{1 - \sin\phi}\,, \tag{3.10}$$

and from the relationship between the initial deformation modulus and the confining pressure, shown in Janbu's (1963) experimental studies,

$$E_{\mathrm{i}} = K p_{\mathrm{a}} \left(\frac{\sigma_3'}{p_{\mathrm{a}}}\right)^n \tag{3.11}$$

an expression determining the tangent deformation modulus E_t:

$$E_{\mathrm{t}} = \left[1 - \frac{R_{\mathrm{f}}(1 - \sin\phi)(\sigma_1 - \sigma_3)}{2c\cos\phi + 2\sigma_3 \sin\phi}\right] \bar{K} p_{\mathrm{a}} \left(\frac{\sigma_3}{p_{\mathrm{a}}}\right)^n \tag{3.12}$$

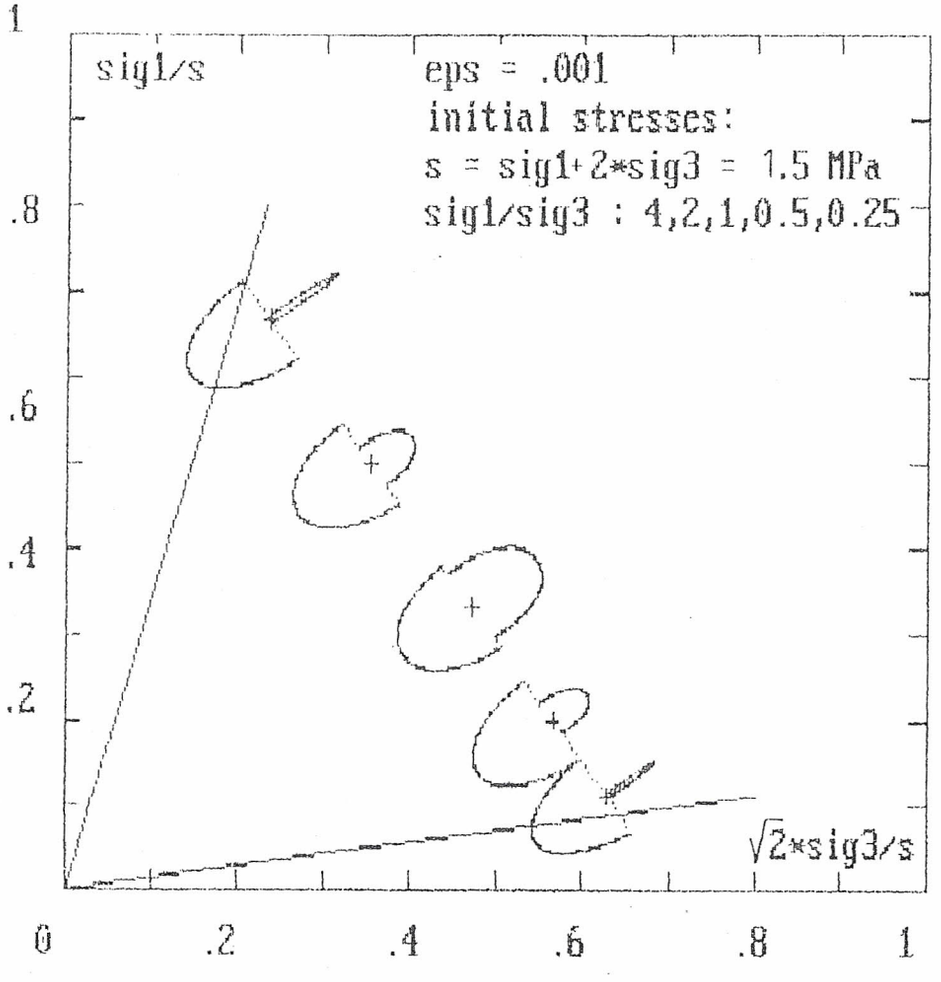

Fig. 5. Bilinear hyperbolic response for different initial states $\sigma_{\mathrm{oct}} = \mathrm{const.}$;
a) switch function: sign $\Delta\sigma_{\mathrm{oct}}$.

This relationship is used only for the first loading. For unloading or reloading a value, computed from the following relationship:

$$E_{\mathrm{ur}} = \bar{K}_{\mathrm{ur}} p_{\mathrm{a}} \left(\frac{\sigma_3}{p_{\mathrm{a}}} \right)^n , \tag{3.13}$$

is assumed.

For determining Poisson's ratio Kulhawy *et al.* (1969) suggested a hyperbolic relationship

$$\varepsilon_1 = \frac{\varepsilon_3}{f + d\varepsilon_3} \tag{3.14}$$

and a relationship accounting for the dependence of Poisson's ratio on the confining pressure:

$$\nu_{\mathrm{i}} = \bar{G} - F \log \left(\frac{\sigma_3}{p_{\mathrm{a}}} \right) \tag{3.15}$$

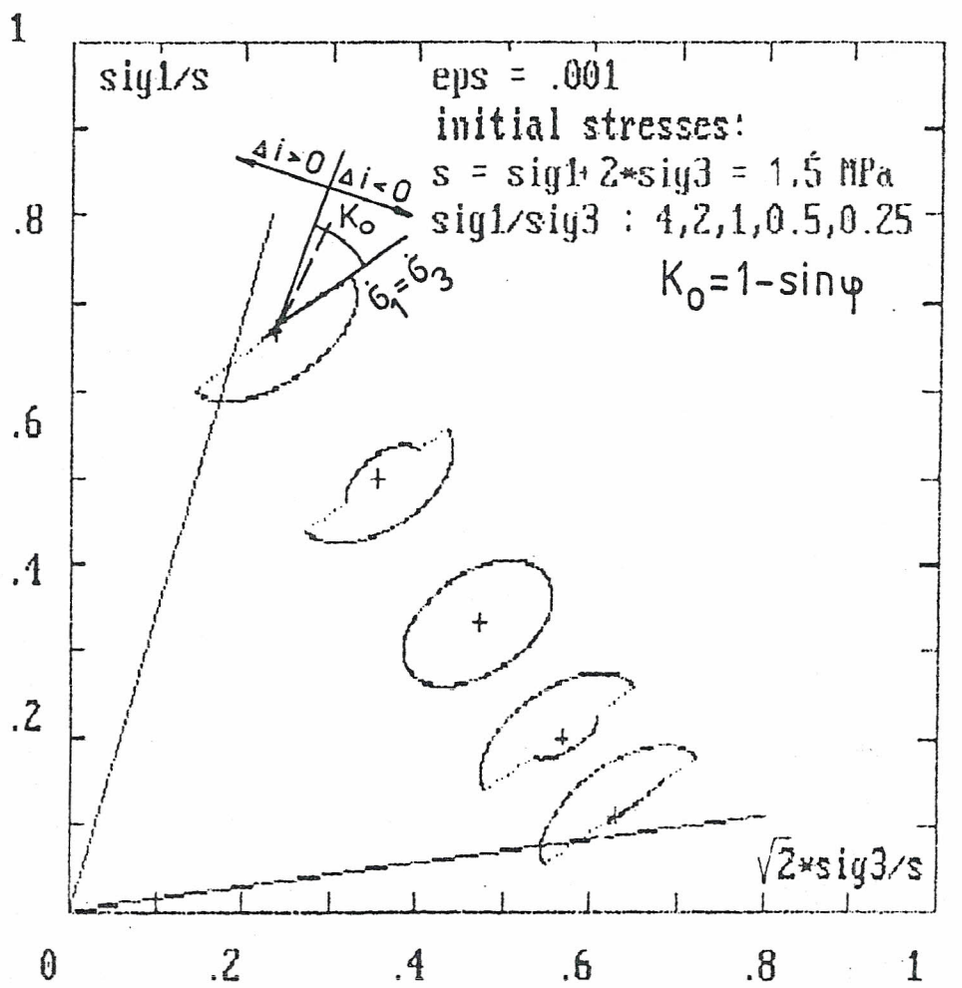

Fig. 5.
b) switch function: sign $(\dot{\varepsilon}_1 - \dot{\varepsilon}_3)$; sig1 $= \sigma_1$, sig3 $= \sigma_3$, eps $= \dot{\varepsilon}$.

Using these relationships, an expression for the tangent Poisson's ratio has been derived:

$$\nu_t = \frac{\bar{G} - F \log\left(\frac{\sigma_3}{p_a}\right)}{\left[1 - \frac{d(\sigma_1 - \sigma_3)}{E_t}\right]^2} \tag{3.16}$$

The deformational $(\bar{K}, \bar{K}_{ur}, n, \bar{G}, f, d)$ and shear strength parameters (c, φ, R_f) appearing in Eqs. (3.10) – (3.16) can be calibrated using standard triaxial test results and procedures according to the above references. Considering the test results given by von Wolffersdorf (1990a, 1990b) the following parameters have been derived for the Karlsruhe sand (initial porosity $e_0 = 0.6111$, contractant part of the stress-strain curve): $\bar{K} = 240, \bar{K}_{ur} = 620, n = 0.85, \bar{G} = 0.25, F = 0.146, d = 8.4, c = 0, \varphi = 41.5°, R_f = 0.8$, atmospheric pressure $p_a = 100$ kPa.

Using these parameters and Eqs. (3.12), (3.13), (3.15) and (3.16), the coefficients M_{ij} determining the shapes of the response envelopes consisting of semi-ellipses, have been calculated. Since no switch functions are given by the authors of the hyperbolic model, either the condition sign $\Delta\sigma_{oct}$ (Fig. 5a) or the function sign $(\dot{\varepsilon}_1 - \dot{\varepsilon}_3)$ (Fig. 5b) can be used. Both series of hyperbolic response envelopes are given in Fig. 5 for identical initial states determined by different stress ratios σ_1/σ_3 and constant mean pressure $\sigma_{oct} = \frac{1}{3}(\sigma_1 + \sigma_2 + \sigma_3) = 0.5$ MPa. One can observe that the loading semi-ellipses with increasing stress ratio have decreasing radius vectors which almost vanish near the limit state. This is due to the decrease of the tangent deformation modulus according to Eq. (3.12).

3.3. Multilinear response

To take into account structural changes of soils induced by different loading paths in a simple way, more than one switch function should be introduced which results in a multilinear response. Strain energy based switch functions can be derived from the rate of work performed by stresses σ_{ij} during an increment of strain $d\varepsilon_{ij}$:

$$dW = \sigma_{ij} d\varepsilon_{ij} \tag{3.17}$$

Introducing the octahedral shear stress component $\tau_{oct} = \frac{1}{3}[(\sigma_1 - \sigma_2)^2 + (\sigma_2 - \sigma_3)^2 + (\sigma_1 - \sigma_3)^2]^{1/2}$, the expression for dW and the corresponding loading $(dW \geq \geq 0)$ and unloading criteria $(dW < 0)$ is given by

$$dW = \frac{3\tau_{oct}}{2G}\, d\tau_{oct} + \frac{\sigma_{oct}}{K}\, d\sigma_{oct} \tag{3.18}$$

where G and K stand for shear and volumetric moduli.

In the path dependent constitutive model suggested by Doležalová (1985), the following criteria and relations have been used for the case of compression $(\sigma_1 > > \sigma_2 > \sigma_3 \geq 0)$:

$$\underline{\Delta\sigma_{\rm oct} \geq 0, \Delta i > 0:}$$

$$E_{\rm t} = E_{\rm p}(\sigma_{\rm oct}/\sigma_0)^{k_1}[1-(1-\delta)\, i_*^{k_2}] \tag{3.19}$$

$$\nu_{\rm t} = \nu_{\rm p} + (\nu_{\rm max} - \nu_{\rm p})\, i_*^{k_3} \tag{3.20}$$

$$\underline{\Delta\sigma_{\rm oct} \geq 0, \Delta i \leq 0:}$$

$$E_{\rm t} = E_{\rm p}(\sigma_{\rm oct}/\sigma_0)^{k_1} \tag{3.21}$$

$$\nu_{\rm t} = \nu_{\rm p} \tag{3.22}$$

$$\underline{\Delta\sigma_{\rm oct} < 0, \Delta i > 0:}$$

$$E_{\rm t} = E_{\rm unl}(\sigma_{\rm oct}/\sigma_0)^{k_1}[1-(1-\delta)\, i_*^{k_2}] \tag{3.23}$$

$$\nu_{\rm t} = \nu_{\rm p} + (\nu_{\rm max} - \nu_{\rm p})\, i_*^{k_3}$$

$$\underline{\Delta\sigma_{\rm oct} < 0, \Delta i \leq 0:}$$

$$E_{\rm t} = E_{\rm unl}(\sigma_{\rm oct}/\sigma_0)^{k_1} \tag{3.24}$$

$$\nu_{\rm t} = \nu_{\rm p}$$

where

$$i_* = (i - i_{\rm p})/(1 - i_{\rm p}) \geq i_{\rm p}\,, \tag{3.25}$$

$$i = \tau_{\rm oct}/\tau_{\rm oct}^{\rm lim}\,, \tag{3.26}$$

$$\tau_{\rm oct}^{\rm lim} = g(\Theta)[N + D\sigma(\sigma_{\rm oct}/\sigma)^B]\,, \tag{3.27}$$

$$g(\Theta) = 2K/[(1+K) - (1-K)\,\sin\,3\Theta]\,, \tag{3.28}$$

$$K = (3 - \sin\varphi)/(3 + \sin\varphi)\,, \tag{3.29}$$

$$-30^\circ < \Theta = \tfrac{1}{3}\sin^{-1}\left(\frac{3\sqrt{3}}{2}\,\frac{J_3}{\bar{\sigma}^3}\right) < +30^\circ\,, \tag{3.30}$$

$$J_3 = (\sigma_1 - \sigma_{\rm oct})(\sigma_2 - \sigma_{\rm oct})(\sigma_3 - \sigma_{\rm oct})\,, \tag{3.31}$$

$$\bar{\sigma} = \sqrt{\tfrac{3}{2}}\,\tau_{\rm oct}\,, \tag{3.32}$$

$$N = 2\sqrt{2}\, c\cos\varphi/(3 - \sin\varphi)\,, \tag{3.33}$$

$$D = 2\sqrt{2}\,\sin\varphi/(3 - \sin\varphi)\,. \tag{3.34}$$

Eqs. (3.33) and (3.34) hold for $B+1$ in Eq. (3.27).

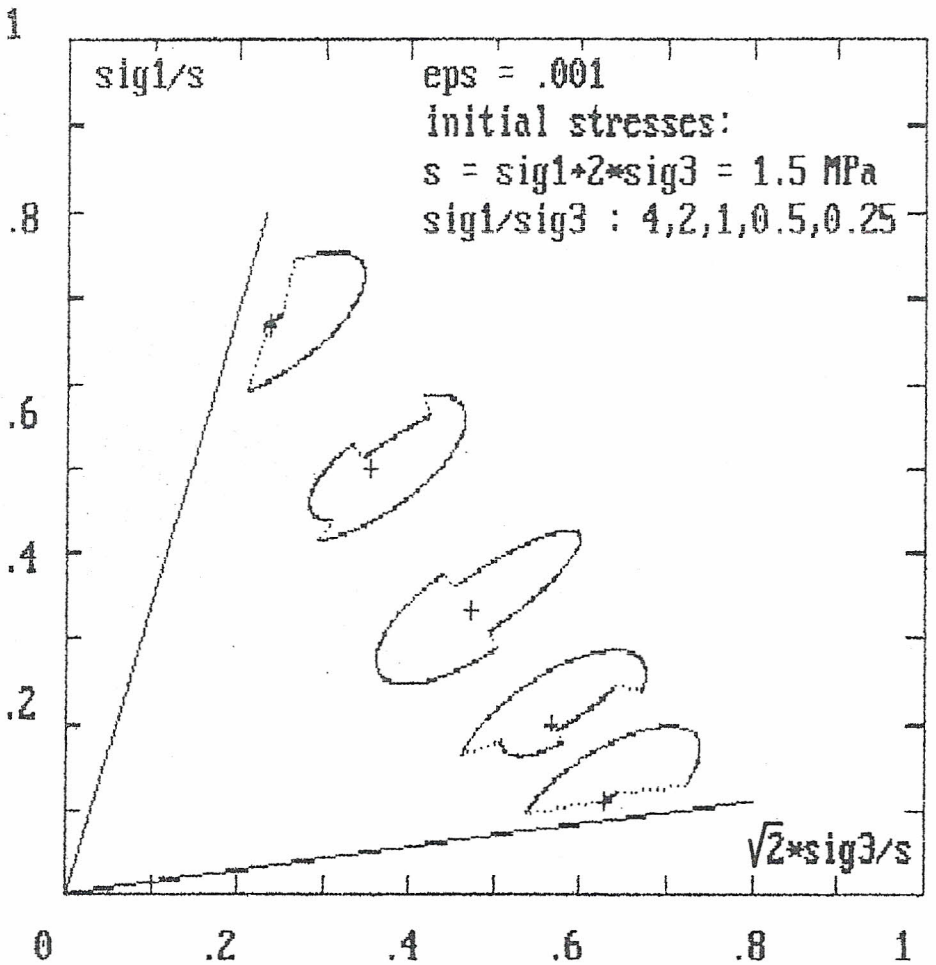

Fig. 6. Multilinear path dependent response for different initial states σ_{oct} = const.; a) ν_t = const.

The tangent deformation modulus E_t and Poisson's ratio ν_t are limited to $E_t \leq$ $\leq E_{max}$ and $\nu_t \leq \nu_{max}$.

The deformation $(E_p, E_{unl}, E_{max}, \nu_p, \nu_{max}, k_1, k_2, k_3, \delta)$ and strength parameters (c, φ) are to be derived from standard triaxial and hydrostatic compression (or oedometric) tests. With the parameters obtained for the Karlsruhe sand (E_p = = 30 MPa, $E_{unl} = 62.14$ MPa, $E_{max} = 100$ MPa, $\nu_p = 0.242, \nu_{max} = 0.45, k_1 = 0.8$, $k_2 = 0.42, k_3 = 0.3, \delta = 0, c = 0, \varphi = 41.5°, i_p = 0.10$ and $\sigma = 1$ MPa, $\sigma_0 = 0.1$ MPa for $e_0 = 0.6111$) the stress response envelopes are shown in Fig. 6. Comparing Figs. 6a and 6b the great influence of the variability of Poisson's ratio on particular paths can be noticed.

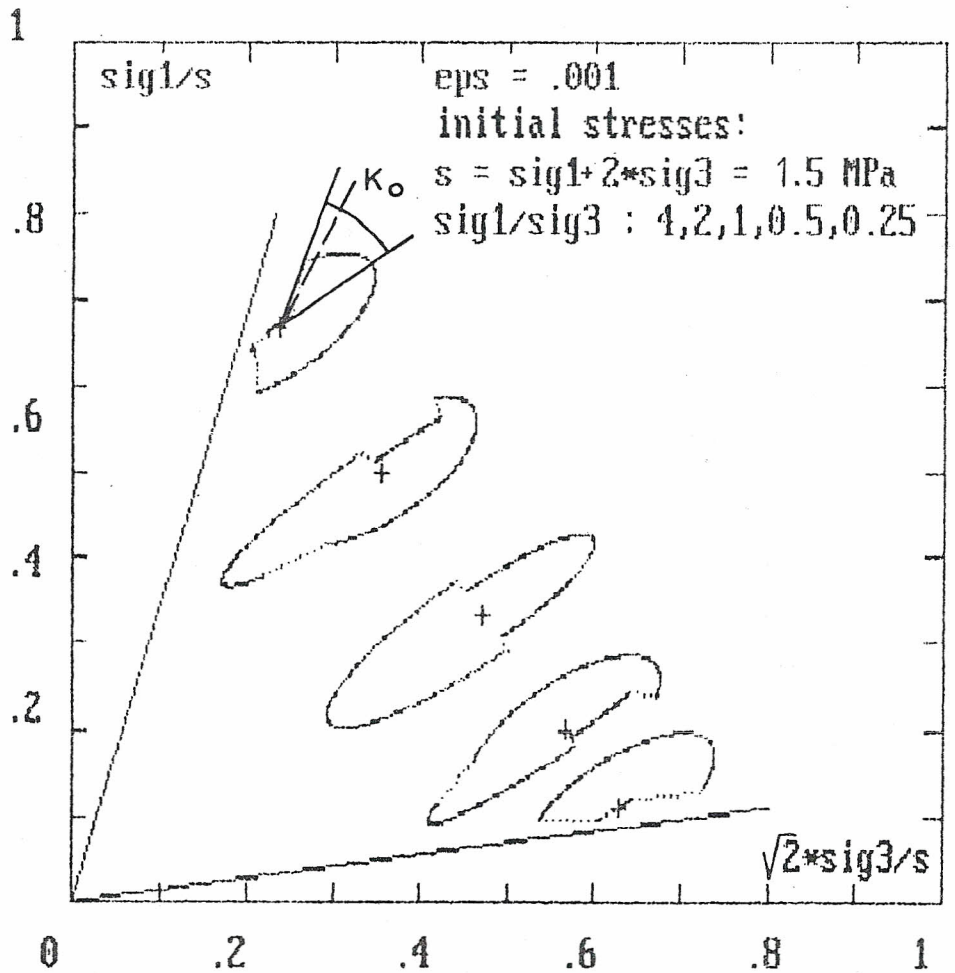

Fig. 6 (continued).
b) $\nu_t \neq$ const. for the stress paths with $\Delta\sigma_{oct} \leq 0$ and $\Delta i > 0$, respectively;
sig1 $= \sigma_1$, sig3 $= \sigma_3$, eps $= \varepsilon$.

4. ELASTOPLASTIC RESPONSE WITH HARDENING

4.1. Formulation of cap models

We shall deal with the formulation of hardening cap models. The modified Cam clay model is described in more detail. Detailed derivation of Cam clay and cap models is presented in Desai and Siriwardane (1984) where it is passed from the results of axially symmetric triaxial tests to the general state of stress. Let us designate the quantities as follows:

$$p = \frac{\sigma_{11} + \sigma_{22} + \sigma_{33}}{3} = \frac{J_1}{3}$$

$$q = \frac{3}{\sqrt{2}}\tau_{\mathrm{oct}} = \frac{1}{\sqrt{2}}[(\sigma_{11}-\sigma_{22})^2 + (\sigma_{22}-\sigma_{33}^2) + (\sigma_{11}-\sigma_{33}^2) +$$

$$+6\sigma_{12}^2 + 6\sigma_{23}^2 + 6\sigma_{13}^2]^{1/2} = \sqrt{3J_{2D}} \tag{4.1}$$

The idea of hardening cap models is based on two yield surfaces, namely, the failure surface F_f and the cap surface F_c depending on material properties and stress history. F_f is fixed in position and the state of stress cannot lie above this critical state of stress. The cap surface F_c moves in dependence on the hardening behaviour of material (Fig. 7). The yield surface F is composed of surfaces F_f and F_c.

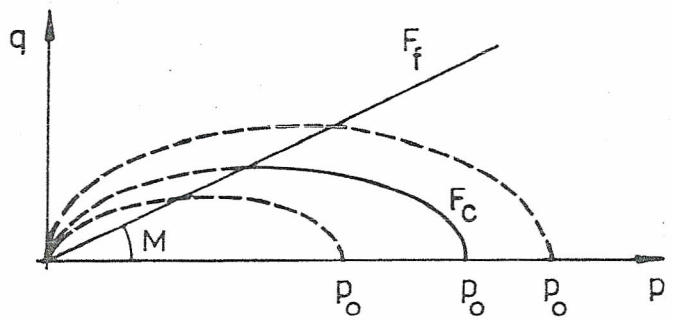

Fig. 7. Failure F_f and hardening F_c surfaces for the critical state (Cam clay) model.

For the modified Cam clay model, it was found that

$$F = q - Mp = 0$$
$$F_c = q^2 - M^2 p p_0 + M^2 p^2 = M^2 J_1^2 - M^2 J_1 J_{01} + 27 J_{2D} = 0 \tag{4.2}$$

where J_1 is the first invariant of the stress tensor and J_{2D} is the second invariant of the deviatoric stress tensor, J_{01} is the value of J_1 at the intersection of F_c with the J_1 axis.

We shall derive the relationship between stress and strain increments. Infinitesimal increments of strain are assumed to be divided into elastic and plastic parts:

$$\mathrm{d}\varepsilon = \mathrm{d}\varepsilon^{\mathrm{e}} + \mathrm{d}\varepsilon^{\mathrm{p}} \tag{4.3}$$

Let $Q = Q(\sigma, p_0)$ be the plastic potential. The normality rule for plastic deformations can be written as

$$\mathrm{d}\varepsilon_{ij}^{\mathrm{p}} = \bar{\lambda}\frac{\partial Q}{\partial \sigma_{ij}} \tag{4.4}$$

where $\bar{\lambda}$ is a non-negative parameter. For the Cam clay model $Q = F$ (associated flow rule).

Let us designate

$$\{\sigma_i\} = (\sigma_{11}, \sigma_{22}, \sigma_{33}, \sigma_{12}, \sigma_{23}, \sigma_{13})^{\mathrm{T}}$$
$$\{\varepsilon_i\} = (\varepsilon_{11}, \varepsilon_{22}, \varepsilon_{33}, \varepsilon_{12}, \varepsilon_{23}, \varepsilon_{13})^{\mathrm{T}}$$

$$\{A_i\} = \left(\frac{\partial Q}{\partial \sigma_{11}}, \frac{\partial Q}{\partial \sigma_{22}}, \frac{\partial Q}{\partial \sigma_{33}}, \frac{\partial Q}{\partial \sigma_{12}}, \frac{\partial Q}{\partial \sigma_{23}}, \frac{\partial Q}{\partial \sigma_{13}}\right)^{\mathrm{T}}$$

$$\{B_i\} = \left(\frac{\partial F}{\partial \sigma_{11}}, \frac{\partial F}{\partial \sigma_{22}}, \frac{\partial F}{\partial \sigma_{33}}, \frac{\partial F}{\partial \sigma_{12}}, \frac{\partial F}{\partial \sigma_{23}}, \frac{\partial F}{\partial \sigma_{13}}\right)^{\mathrm{T}}, \quad i = 1, \ldots, 6$$

$$\varepsilon_\nu = \varepsilon_{11} + \varepsilon_{22} + \varepsilon_{33} - \text{volumetric strain}$$

Let $\mathbf{C}^{\mathrm{e}}$ be the elastic matrix. Using (4.3) and (4.4) we have

$$\mathrm{d}\sigma_i = C^{\mathrm{e}}_{ij}(\mathrm{d}\varepsilon_j - \mathrm{d}\varepsilon^{\mathrm{p}}_j) = C^{0}_{ij}(\mathrm{d}\varepsilon_j - \bar{\lambda} A_j) \tag{4.5}$$

During plastic deformation $F(\sigma, p_0) = 0$ and, hence, by differentiation:

$$\mathrm{d}F = \frac{\partial F}{\partial \sigma_{11}}\,\mathrm{d}\sigma_{11} + \cdots + \frac{\partial F}{\partial \sigma_{13}}\,\mathrm{d}\sigma_{13} + \frac{\partial F}{\partial p_0}\,\mathrm{d}p_0 = 0 \tag{4.6}$$

For the Cam clay model, the hardening parameter p_0 depends on the plastic part of the volumetric strain $\varepsilon^{\mathrm{p}}_\nu$, hence $p_0 = p_0(\varepsilon^{\mathrm{p}}_\nu)$. In equation (4.6), it can be substituted for

$$\frac{\partial F(\sigma, p_0)}{\partial p_0}\,\mathrm{d}p_0 = \frac{\partial F(\sigma, p_0(\varepsilon^{\mathrm{p}}_\nu))}{\partial p_0}\,\frac{\partial p_0}{\partial \varepsilon^{\mathrm{p}}_\nu}\,\mathrm{d}\varepsilon^{\mathrm{p}}_\nu = \frac{\partial F(\sigma, p_0(\varepsilon^{\mathrm{p}}_\nu))}{\partial \varepsilon^{\mathrm{p}}_\nu}\,\mathrm{d}\varepsilon^{\mathrm{p}}_\nu$$

Substituting (4.4) and (4.5) in (4.6) we obtain

$$\begin{aligned}\mathrm{d}F &= B_i C^{\mathrm{e}}_{ij}(\mathrm{d}\varepsilon_j - \bar{\lambda} A_j) + \frac{\partial F}{\partial \varepsilon^{\mathrm{p}}_\nu}\,\mathrm{d}\varepsilon^{\mathrm{p}}_\nu = \\ &= B_i C^{\mathrm{e}}_{ij}(\mathrm{d}\varepsilon_j - \bar{\lambda} A_j) + \frac{\partial F}{\partial \varepsilon^{\mathrm{p}}_\nu}\,\bar{\lambda}(A_1 + A_2 + A_3)\end{aligned} \tag{4.7}$$

Equation (4.7) yields

$$\bar{\lambda} = \frac{B^{\mathrm{T}}_k C^{\mathrm{e}}_{kj} A_j}{B^{\mathrm{T}}_k C^{\mathrm{e}}_{kj} A_j - \dfrac{\partial F}{\partial \varepsilon^{\mathrm{p}}_\nu}\,(A_1 + A_2 + A_3)} \tag{4.8}$$

Substitution for $\bar{\lambda}$ in (4.5) yields the required relationship between stress and strain (in incremental form):

$$\mathrm{d}\sigma_i = \left[C^{\mathrm{e}}_{ij} - \frac{C^{\mathrm{e}}_{ik} A_k B^{\mathrm{T}}_m C^{\mathrm{e}}_{mj}}{B^{\mathrm{T}}_k C^{\mathrm{e}}_{kj} A_j - \dfrac{\partial F}{\partial \varepsilon^{\mathrm{p}}_\nu}\,(A_1 + A_2 + A_3)}\right] \mathrm{d}\varepsilon_j = C^{\mathrm{ep}}_{ij}\,\mathrm{d}\varepsilon_j \tag{4.9}$$

Equation (4.9) defines the elastoplastic constitutive matrix $\mathbf{C}^{\mathrm{ep}}$.

The form of all terms in (4.9) will be given for the modified Cam clay model. As $F = Q$, we can compute for instance $\{A_i\}$. Defining $K = \frac{1}{2}M^2(2p - p_0)$ we obtain

$$\{A_i^T\} = \begin{Bmatrix} K + 2\sigma_{11} - \sigma_{22} - \sigma_{33} \\ K + 2\sigma_{22} - \sigma_{11} - \sigma_{33} \\ K + 2\sigma_{11} - \sigma_{22} - \sigma_{33} \\ 6\sigma_{12} \\ 6\sigma_{23} \\ 6\sigma_{13} \end{Bmatrix}$$

It has been derived

$$\frac{\partial F}{\partial \varepsilon_v^p} = -\frac{M^2 p p_0 (1 + e_0)}{\lambda - k} \tag{4.10}$$

where e_0 is the void ratio prior to a stress increment, and the meaning of λ and k is obvious from Fig. 8. In the same way, p and p_0 are quantities related to F_c

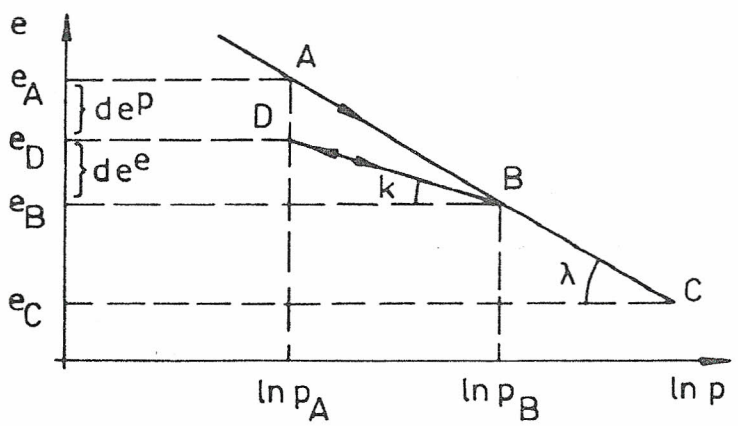

Fig. 8. Isotropic loading and unloading in e—ln p space.

prior to a stress increment. The change in the void ratio $de = de^e + de^p$ has been determined as

$$de = -\lambda \frac{dp_0}{p_0} \tag{4.11}$$

$$de^e = -k \frac{dp_0}{p_0} \tag{4.12}$$

Equations (4.11) and (4.12) hold true for $q = 0$. The value of dp_0 can be expressed from (4.2) by substitution of p and q after an increment.

For a general value of q, de can be expressed as ($\mu = q/p$):

$$de = -(1 + e_0)\, d\varepsilon_v = -\lambda \left[\frac{dp}{p} + \left(1 - \frac{k}{\lambda}\right) 2 \frac{\mu d\mu}{M^2 + \mu^2} \right] \tag{4.13}$$

All the terms in (4.9) are thus given for the modified Cam clay model.

The mere formulation of elastoplastic models is insufficient to solve boundary value problems with non-linear stress-strain relationships. The determination of the elastoplastic stress increment at a given stress point requires further effort and this is the topic of the next section.

4.2. Computational procedures for implementing hardening models at one stress point

This part makes use of the results of Sirwardane and Desai (1983). Two yield surfaces form two criteria. The incremental stress corresponding to an increment of strain can violate one or both of the criteria. Hence, these possibilities have to be checked at all stress points in implementing elastoplastic hardening models.

For an increment of strain, $d\varepsilon$, the corresponding $d\sigma$ can be computed by using (4.9). If the final state of stress lies within or on the yield and failure surfaces, the following criteria have to be satisfied:

$$F_c(\sigma_0 + d\sigma) \leq 0 \tag{4.14a}$$

$$F_f(\sigma_0 + d\sigma) \leq 0 \tag{4.14b}$$

where σ_0 is the state of stress prior to an increment. The possibilities of violating the two criteria (4.14) are shown in Fig. 9.

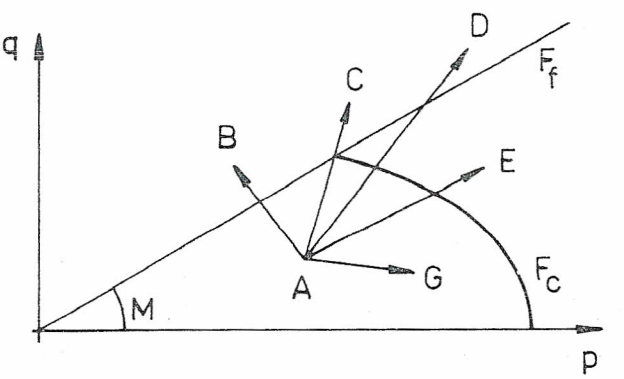

Fig. 9. Possible stress increments for loading from an elastic point.

The path AB intersects F_f directly from the elastic region, AC and AD from the plastic region. Since the state of stress above F_f cannot exist, it is necessary to find the increment of stress $\Delta\sigma$ which will bring the stress point to the failure state. The material is unable to bear any more stress, and hence an unbalanced load fraction arises. Solving boundary value problems by FEM this is redistributed to the surrounding elements by using iterative methods.

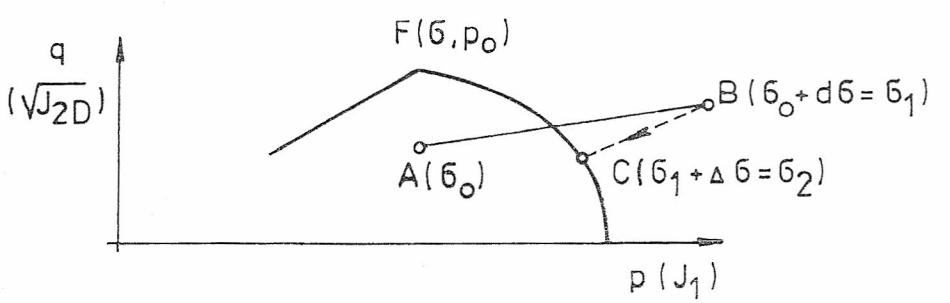

Fig. 10. Stress correction along the normal to the yield surface F.

We shall correct the stress by bringing the stress point B along the normal to general surface F. This procedure can be applied both to F_f and F_c (Fig. 10).

The change of $F(\sigma, p_0)$ can be expressed as (p_0 is fixed)

$$dF = F(\sigma_0 + d\sigma + \Delta\sigma) - F(\sigma_0 + d\sigma) \equiv \frac{\partial F(\sigma_0 + d\sigma)}{\partial \sigma_{ij}} \Delta\sigma_{ij} \tag{4.15}$$

Let us designate $F_1 = F(\sigma_0 + d\sigma)$, $\sigma_1 = \sigma_0 + d\sigma$. Equation (4.15) in matrix form yields

$$0 - F_1 = \left\{ \frac{\partial F(\sigma_1)}{\partial \sigma} \right\}^{\mathrm{T}} \{\Delta\sigma\} \tag{4.16}$$

From here the change of stress $\{\Delta\sigma\}$ bringing σ_1 along the normal to surface F can be expressed as

$$\{\Delta\sigma\} = \frac{\left\{ -F_1 \dfrac{\partial F(\sigma_1)}{\partial \sigma} \right\}}{\left\{ \dfrac{\partial F(\sigma_1)}{\partial \sigma} \right\}^{\mathrm{T}} \left\{ \dfrac{\partial F(\sigma_1)}{\partial \sigma} \right\}} \tag{4.17}$$

As the value of $\partial F/\partial\sigma$ is calculated at a point outside F, it need not be exactly normal to F, and hence $\sigma_1 + \Delta\sigma$ need not lie on F. Stress point $\sigma_2 = \sigma_1 + \Delta\sigma$ can be used as the further approximation of this algorithm and value $\sigma_3 = \sigma_2 + \Delta\sigma$ can be calculated according to (4.17), and so on, until $\sigma_{k+1} = \sigma_k + \Delta\sigma$ falls within the prescribed accuracy.

Let us go back to Fig 9. Paths AD and AE enter the region of elastoplastic deformations. The final state of stress is computed by gradual expanding F_c, as described below.

The violation of (4.14a) is dealt with. The increment of stress computed from the elastic matrix can move the state of stress outside the actual F_c (see Fig. 11). Until the state of stress reaches the stress point C, the material deforms elastically.

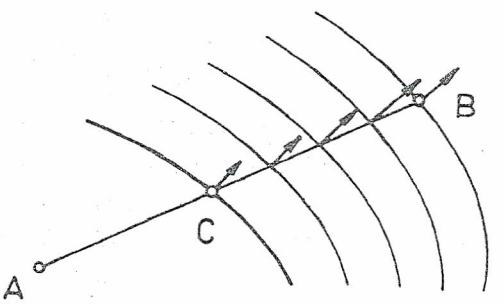

Fig. 11. Transition to the plastic region with expanding yield caps for subincrements of strain $(1-S)\ d\varepsilon/m$.

The determination of C will be described later. Constant S divides an increment of stress into elastic and elastoplastic parts:

$$\{d\sigma\} = S[\mathbf{C}^{\mathrm{e}}]\{d\varepsilon\} + (1 - S)[\mathbf{C}^{\mathrm{ep}}]\{d\varepsilon\} = \{d\sigma^{\mathrm{e}}\} + \{d\sigma^{\mathrm{ep}}\} \tag{4.18}$$

The incremental stress corresponding to the incremental strain has to be computed separately for elastic and elastoplastic behaviour (indices e and ep):

$$\{\mathrm{d}\sigma^{\mathrm{e}}\} = S[\mathbf{C}^{\mathrm{e}}]\{\mathrm{d}\varepsilon\} = [\mathbf{C}^{\mathrm{e}}]\{\mathrm{d}\varepsilon^{\mathrm{e}}\} \tag{4.19}$$

$$\{\mathrm{d}\sigma^{\mathrm{ep}}\} = (1-S)[\mathbf{C}^{\mathrm{ep}}]\{\mathrm{d}\varepsilon\} = [\mathbf{C}^{\mathrm{ep}}]\{\mathrm{d}\varepsilon^{\mathrm{ep}}\} \tag{4.20}$$

The computation of $\{\sigma^{\mathrm{e}}\}$ is straightforward once S is determined. However, the evaluation of $\{\sigma^{\mathrm{ep}}\}$ requires $(1-S)\{\mathrm{d}\varepsilon\}$ to be divided into m subincrements, the value of m being given by the ratio of the increment of the hardening parameter $\mathrm{d}p_0$ (corresponding to states of stress B and C in Fig. 11) to the highest allowed increment ΔF : $\mathrm{d}p_0/\Delta F$. It is important to point out the fact that F_{c} changes its position after each subincrement $(1-S)\{\mathrm{d}\varepsilon\}/m$ has been applied.

The hardening parameter, p_0, and void ratio e_0 are updated together with the stress increment corresponding to each subincrement of strain $(1-S)\mathrm{d}\varepsilon/m$ (see (4.2), (4.11)–(4.13)). The state of stress has to lie on the actual surface F_{c}. There are two possible ways of updating p_0. The value of p_0 can be determined either from equation (4.2) (p and q are known, $F_{\mathrm{c}} = 0$) or from equations (4.11) and (4.13) (if $F_{\mathrm{c}} \neq 0$, the state of stress is brought to F_{c} using the procedure described in (4.15)–(4.17)). If subincrements $(1-S)\mathrm{d}\varepsilon/m$ are sufficiently small, both ways yield the same results.

The critical state can be reached in computing the m subincrements (path AD in Fig. 9). Hence the violation of (4.14b) has to be checked after each subincrement. If $F_{\mathrm{f}} > 0$ holds true, the correction to bring the state of stress along the normal to F_{f} is applied.

The correct value of $\{\mathrm{d}\sigma^{\mathrm{ep}}\}$ is the accumulated quantity over the m subincrements. If the critical state is reached after k subincrements ($k < m$), the iteration is stopped and the correct value of $\{\mathrm{d}\sigma^{\mathrm{ep}}\}$ is calculated by adding k subincrements. We can thus determine $\{\mathrm{d}\sigma\}$ in (4.18).

Let us outline the procedure for evaluating S. This can be done by solving the quadratic equation (e.g. for the modified Cam clay model) or in a general case by using an iterative procedure similar to (4.15)–(4.17) (see Nayak and Zienkiewicz, 1972). For the modified Cam clay model, S can be determined as follows.

Equation $F_{\mathrm{c}}(\sigma_0 + S\mathrm{d}\sigma) = 0$ is to hold true. Substituting this in (4.2) we obtain quadratic equation $AS^2 + BS + C = 0$ with

$$\begin{aligned} A &= 27\mathrm{d}J_{2\mathrm{D}} + M^2\mathrm{d}J_1^2 \\ B &= 54a - M^2 J_{01}\mathrm{d}J_1 + 2M^2 J_1^2\mathrm{d}J_1 \\ C &= 27J_{2\mathrm{D}} - M^2 J_1 J_{01} + M^2 J_1^2 \end{aligned}$$

$$\begin{aligned} a = \tfrac{1}{6}\{&(\sigma_{11}-\sigma_{22})(\mathrm{d}\sigma_{11}-\mathrm{d}\sigma_{22}) + (\sigma_{22}-\sigma_{33})(\mathrm{d}\sigma_{22}-\mathrm{d}\sigma_{33}) + \\ &+ (\sigma_{11}-\sigma_{33})(\mathrm{d}\sigma_{11}-\mathrm{d}\sigma_{33})\} + \sigma_{12}\mathrm{d}\sigma_{12} + \sigma_{23}\mathrm{d}\sigma_{23} + \sigma_{13}\mathrm{d}\sigma_{13} \end{aligned}$$

where $\mathrm{d}J_{2\mathrm{D}}$ and $\mathrm{d}J_1$ are invariants of the incremental stress $\mathrm{d}\sigma$.

So far loading has been involved. After yielding or reaching a critical state, the state of stress can indicate unloading (see Fig. 12). If this is the case, the computed stress increments are assumed to be correct, and the unloading constitutive parameters are assigned at those stress points for subsequent unloading. By definition unloading is elastic.

With the parameters obtained for the Karlsruhe sand ($M = 1.715, \lambda = 0.01036$,

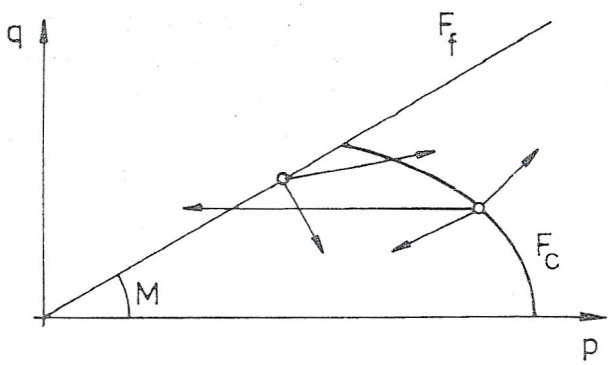

Fig. 12. Possible unloading paths after reaching the failure F_f or yield surface F_c.

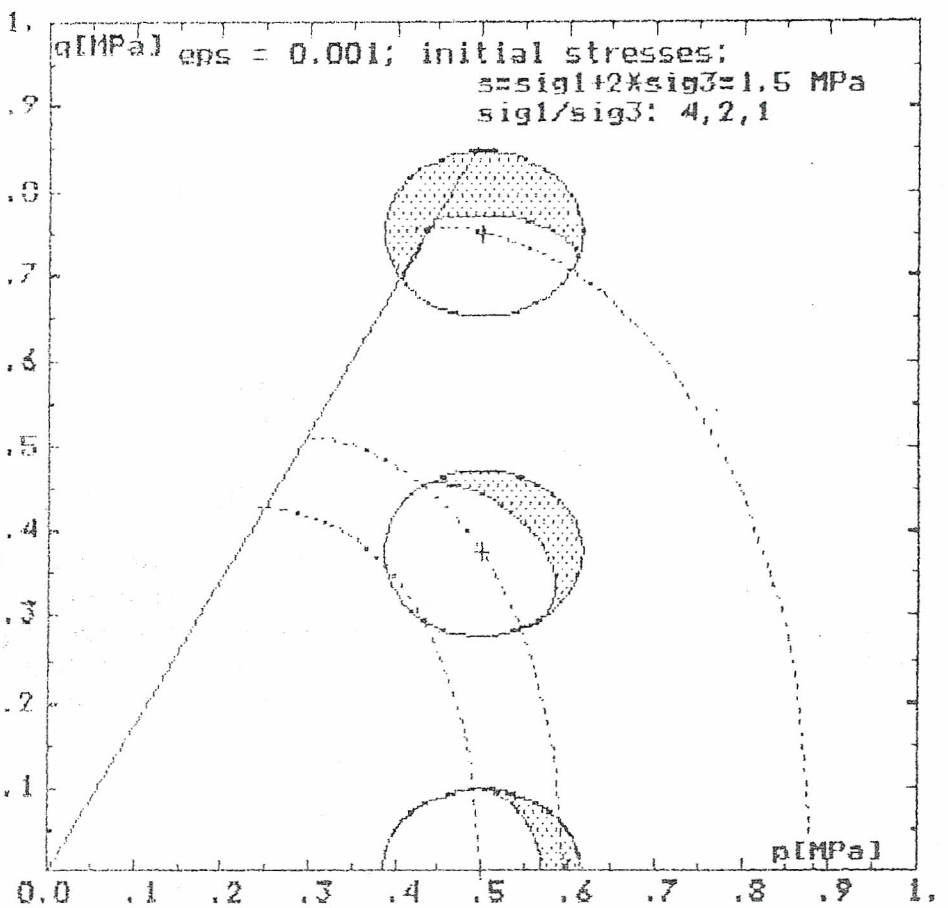

Fig. 13. Response envelopes of the critical state model for different initial states $\sigma_{oct} = \text{const.}$; a) in $q - p$ space.

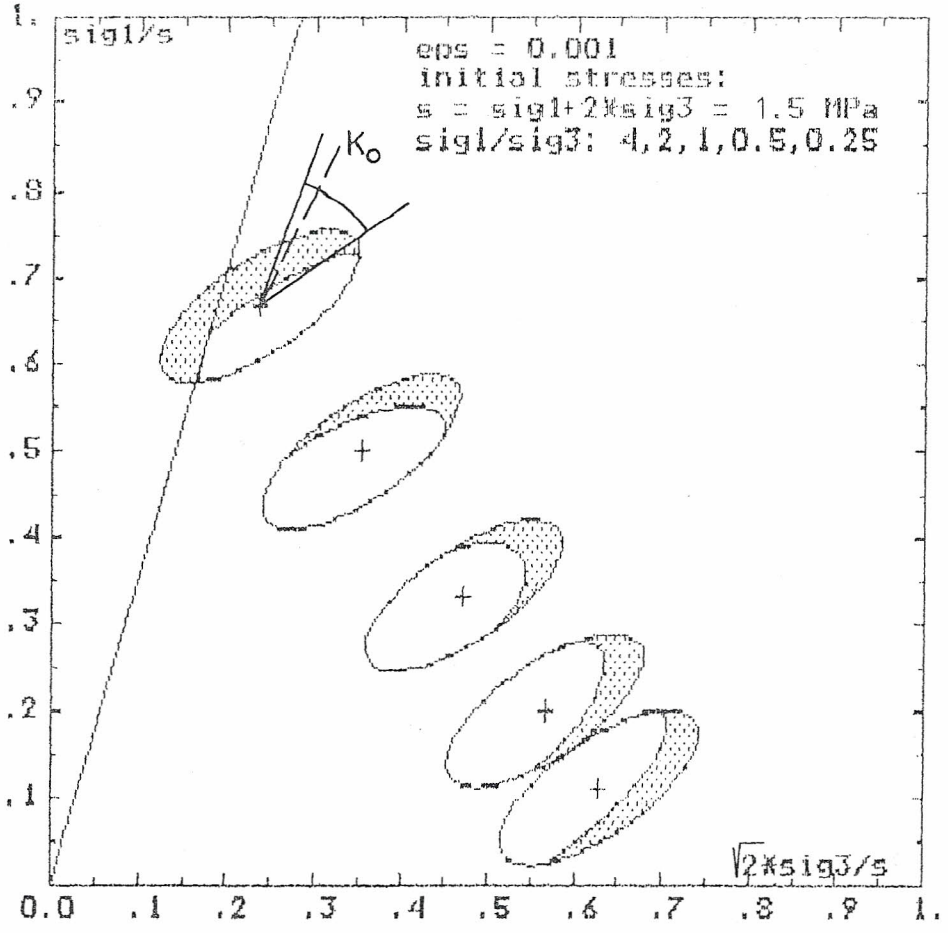

Fig. 13 (continued).

b) in $\sigma_1 - \sqrt{2}\,\sigma_3$ space; sig1 $= \sigma_1$, sig3 $= \sigma_3$, eps $= \varepsilon$.

$k = 0.00197, e_0 = 0.6111, p = 0.5$ MPa, $E = 100$ MPa, $\nu = 0.25, c = 0, \varphi = 41.83°$) the critical state or Cam clay model response is shown in Figs. 13a and 13b. The different shapes of the response envelopes in these figures correspond to the different spaces ($q - p$ and $\sigma_1 - \sqrt{2}\,\sigma_2$) used. The shaded areas of the response envelopes indicate the difference between the pure elastic and the elastoplastic responses. It should be noted that for computing the unit stress response envelopes $S = 0$ holds.

5. COMPARISON OF THE MODELS

The response envelopes allow rapid discrimination and evaluation of both the physical and mathematical aspects of particular constitutive models. One can easily realize the effect of selected switch functions or material parameters. Regarding space limitation, however, only a few remarks are made here.

The important condition of response envelope continuity is satisfied by the linear elastic models (Figs. 3 and 4), but this response does not match the real behaviour of geomaterials. The response of the hyperbolic model is fairly discontinuous and depends considerably on the selected switch function (Figs. 5a and 5b). The

path dependent model also displays discontinuous response controlled by the switch functions. The continuous response of the elastoplastic critical state model (Figs. 13a, b) proves that this model is mathematically considerably better posed than the preceding variable moduli models.

Concerning the physical correctness of the tested nonlinear models, the hyperbolic response with the switch function sign $(\varepsilon_1 - \varepsilon_3)$ (Fig. 5b) is more realistic than the response with the alternative switch function in Fig. 5a. Similarly, for the paths where loading in shear occurs $(\Delta i > 0)$ the multilinear response of the path dependent model with $\nu \neq 0$ (Fig. 6b) is more correct than its response with $\nu = \text{const.}$ in Fig. 6a. The comparable Cam clay model is plotted in Fig. 13b. All these models simulate the standard triaxial test paths with $\dot{\sigma}_3 = \text{const.}$ or $\dot{\sigma}_{\text{oct}} = \text{const.}$ well, i.e. the above-mentioned paths with loading in shear. The difference between the models can only be established by more complicated tests, e.g. by a sudden change of path direction due to unloading in shear $(\Delta i \leq 0)$. This stress path group noted for a significant stiffening effect (Doležalová and Hoření, 1982) is shown in Figs. 5b, 6b and 13b. It can be said that only the path dependent model takes into account this effect which is of great importance for realistic displacement prediction of geotechnical structures.

6. CONCLUSION

The numerical element tests and unit stress response envelopes have proved to be powerful tools for numerical testing of incremental constitutive relations of geomaterials. The physical and mathematical aspects of the particular relations can be easily compared and understood. Furthermore, the effect of various switch conditions and material parameters can be simply visualized. In this way quick and inexpensive parametric studies can be carried out for both the right choice of the constitutive model and the check of selected parameters of particular materials. Such a parametric study should precede any FEM analysis of a real geotechnical structure.

Concerning the future research specification of detailed conditions to be imposed on constitutive models, testing of other elastoplastic and rate type relations, and implementation of some selected relations in the FEM codes are planned. The next step, according to the accepted grant project, is the solution of some typical boundary value problems using different constitutive laws and their comparison with the field measurement results.

REFERENCES

Beer, G., J.R. Booker and J.P. Carter (1991). Computer Methods and Advances in Geomechanics. Chapter 6: Constitutive Modelling, in *Proceedings of 7th IACMAG Conference,* Cairns, Vol. 1, 535-723.

Bojtár, I. (1988). *Mechanical Material Models,* Tankönyvkiadó, Budapest, 290 pp. (in Hungarian).

Desai, C.S. and H.J. Siriwardane (1984). *Constitutive Laws for Engineering Materials with Emphasis on Geological Materials*, Prentice-Hall, Inc., Englewood Cliffs, 471 pp.

Doležalová, M. (1985). Description of a pseudoelastic constitutive model, in *Proc. of Conf. on "Use of microcomputers for solving soil mech. and found. eng. problems"*, Prague, 130–141 (in Czech).

Doležalová, M. and A. Hoření (1982). A Path Dependent Computational Model for Rockfill Dams, in *Int. Symp. on Num. Models in Geomechanics*, Zurich, 577-586.

Duncan, J. N. and C.Y. Chang (1970). Nonlinear Analysis of Stress and Strain in Soils, *J. Soil Mech. Found. Div. ASCE* **96**, No. SM5, 1629–1653.

Feda, J. (1982). *Mechanics of Particulate Materials. The Principles*, Academia, Prague, 447 pp.

Gudehus, G. (1979). A comparison of some constitutive laws for soils under radially symmetric loading and unloading, in *3rd Int. Conf. on Numerical Methods in Geomechanics*, Aachen, 1309–1323.

Gudehus, G. (1985). Requirements for Constitutive Relations for Soils. Chapter 4 in *Mechanics of Geomaterials*, edited by Z. Bazant, John Wiley and Sons Ltd, 47–63.

Gudehus, G., F. Darveand and I. Vardoulakis, (1984). *Constitutive Relations of Soils – Results of a Workshop*, Balkema, Rotterdam, 497 pp.

Gudehus, G. and D. Kolymbas (1985). Numerical testing of constitutive relations for soils, in *5th Int. Conf. on Numerical Methods in Geomechanics*, Nagoya, 63–81.

Janbu, N. (1963). Soil Compressibility as Determined by Oedometer and Triaxial Test, in *Proc. of Eur. Conf. Soil Mech. Found. Eng.*, Wiesbaden, Vol. 1, 19–25.

Kolymbas, D. (1987). A Constitutive Law of the Rate Type for Soils and Other Granular Materials, in *1st Czechoslovak Conf. on Num. Meth. in Geomechanics*, Vysoké Tatry, Vol. 1, 70–86.

Kondner, R.L. (1963). Hyperbolic Stress-Strain Response: Cohesive Soils, *ASCE* **89**, SM1, 115–143.

Kulhawy, F.H., J.M. Duncan and H.B. Seed (1969). Finite Element Analysis of Stresses and Movements in Embankments during Construction, *Rep. 569-8*, U.S. Army Corps of Engineers Waterways Exp. Str., Vicksburg.

Leigh, D. C. (1968). *Nonlinear Continuum Mechanics*, McGraw-Hill, New York, 240 pp.

Murayama, S. (1984). *Preliminary Draft of State-of-the-art on Constitutive Laws of Soils*, ISSMFE Japanese Local Task Committee, Kyoto, Japan.

Nayak, G.C. and O.C. Zienkiewicz (1972). Elasto-plastic Stress Analysis. Generalization for Various Constitutive Laws Including Strain Softening, *Int. J. Num. Meth. Eng.* **5**, 113–135.

Roscoe, K. H., A. Schofield and C.P. Worth (1958). On the Yielding of Soils, *Géotechnique* **8**, 22–53.

Siriwardane, H.J. and C.S. Desai (1983). Computational Procedures for Non-linear 3D Analysis with Some Advanced Constitutive Laws, *Int. J. Num. An. Meth. Geom.* **7**, 143–171.

Truesdell, C. (1984). *Rational Thermodynamics*, 2nd Edition, Springer-Verlag, New York, 578 pp.

Wolffersdorf, P.A. von (1990a). *Documents of laboratory and field tests for bearing capacity predictions for "Baugrundtagung: 1990"*, Institut für Bodenmechanik und Grundbau, Universität Karlsruhe, Personal communication.

Wolffersdorf, P.A. von (1990b). Probebelastung zur Baugrundtagung 1990: Bodedaten, *Geotechnik*, 44–46.

NUMERICKÉ TESTOVÁNÍ A POROVNÁNÍ KONSTITUTIVNÍCH MODELŮ GEOMATERIÁLŮ

Marta Doležalová, Zdeněk Boudík a Ivo Hladík

Numerické testování a grafické zobrazování hypoelastických konstitutivních vztahů geomateriálů užitím elementárních numerických testů a jednotkové napěťové odezvy podle Gudehuse (1979). Odvození základních vztahů a srovnání pěti modelů: izotropního lineárně elastického, transverzálně izotropního, hyperbolického s různými přepínacími funkcemi, dráhově závislého (variable moduli) a elastoplastického (Cam clay) modelu se zpevněním.

Received 17 September 1991